Bone Reports 14 (2021) 100740

Contents lists available at ScienceDirect

Bone Reports

journal homepage: www.elsevier.com/locate/bonr

The investigation of bone fracture healing under intramembranous and endochondral ossification

Smriti Ghimire [a,*], Saeed Miramini [a], Glenn Edwards [b], Randi Rotne [b], Jiake Xu [c], Peter Ebeling [d], Lihai Zhang [a]

[a] Department of Infrastructure Engineering, The University of Melbourne, Victoria 3010, Australia
[b] School of Animal & Veterinary Sciences, Charles Sturt University, NSW 2678, Australia
[c] School of Pathology and Laboratory Medicine, University of Western Australia, WA 6009, Australia
[d] Department of Medicine, Monash University, Clayton, Victoria 3168, Australia

ARTICLE INFO

Keywords:
Bone fracture healing
Mechano-regulation
Intramembranous ossification
Endochondral ossification
Locking compression plate
Titanium

ABSTRACT

After trauma, fractured bone starts healing directly through bone union or indirectly through callus formation process. Intramembranous and endochondral ossification are two commonly known mechanisms of indirect healing. The present study investigated the bone fracture healing under intramembranous and endochondral ossification by developing theoretical models in conjunction with performing a series of animal experiments. Using experimentally determined mean bone densities in sheep tibia stabilized by the Locking Compression Plate (LCP) fixation system, the research outcomes showed that intramembranous and endochondral ossification can be described by Hill Function with two unique sets of function parameters in mechanical stimuli mediated fracture healing. Two different thresholds exist within the range of mechanical simulation index which could trigger significant intramembranous and endochondral ossification, with a relatively higher bone formation rate of endochondral ossification than that of intramembranous ossification. Furthermore, the increase of flexibility of the LCP system and the use of titanium LCP could potentially promote uniform bone formation across the fracture gap, ultimately better healing outcomes.

1. Introduction

Bone fractures can occur under traumatic (e.g. sport injuries or traffic accidents) or non-traumatic condition (e.g. osteoporosis and bone cancer) (Moroni et al., 2005; Rodan and Martin, n.d.). Primary bone healing is a direct bone union process (also referred to as intramembranous ossification), which takes place on a very small fracture gap (order of 10-100 μm) with strain under 2%, and often requires a rigid fixation like a conventional compression plate in place to maintain absolute stability of the fracture site for much longer time, even years (McKibbin, 1978). In contrast, secondary healing is indirect healing (mainly endochondral ossification), which is more common and occurs in fracture gaps with larger micro motions and can be achieved by increasing the flexibility of fixation system like locking plates (Perren, 2002; Woo et al., 1983). During endochondral ossification cartilage is formed, calcified and finally replaced by bone; whereas in intramembranous ossification, bone tissue is directly synthesized by osteoblasts formed through mesenchymal stem cell differentiation (MSC) (Doblaré et al., 2004). It is important to note that in case of secondary healing, both endochondral and intramembranous ossification can occur within a single fracture depending on strain and vascularity level at different zones of fracture site (Ghiasi et al., 2017; Baker et al., 2018; Gerstenfeld et al., 2003). Previous studies (Einhorn, 1998; Marsell and Einhorn, 2011) show that endochondral ossification occurs between fractured bone and external to periosteal callus (under relatively large strain), while intramembranous ossification occurs simultaneously in callus away from fracture site directly adjacent to distal and periosteal end of cortex (under relatively low strain). Direct and indirect healing have been qualitatively studied (Augat et al., 1998; Perren, 1979; Vetter et al., 2010), and the fundamental mechano-regulation principles governing tissue differentiation has been investigated through finite element methods as well as experiments (Claes et al., 1995; Gardner et al., 2006; Gardner and Mishra, 2003; Lacroix and Prendergast, 2002). Through rat experiments, Morgan et al. (2010) and

* Corresponding author.
E-mail addresses: smritig@student.unimelb.edu.au (S. Ghimire), s.miramini@unimelb.edu.au (S. Miramini), rrotne@csu.edu.au (R. Rotne), jiake.xu@uwa.edu.au (J. Xu), peter.ebeling@monash.edu (P. Ebeling), lihzhang@unimelb.edu.au (L. Zhang).

https://doi.org/10.1016/j.bonr.2020.100740
Received 7 August 2020; Received in revised form 7 December 2020; Accepted 11 December 2020
Available online 15 December 2020

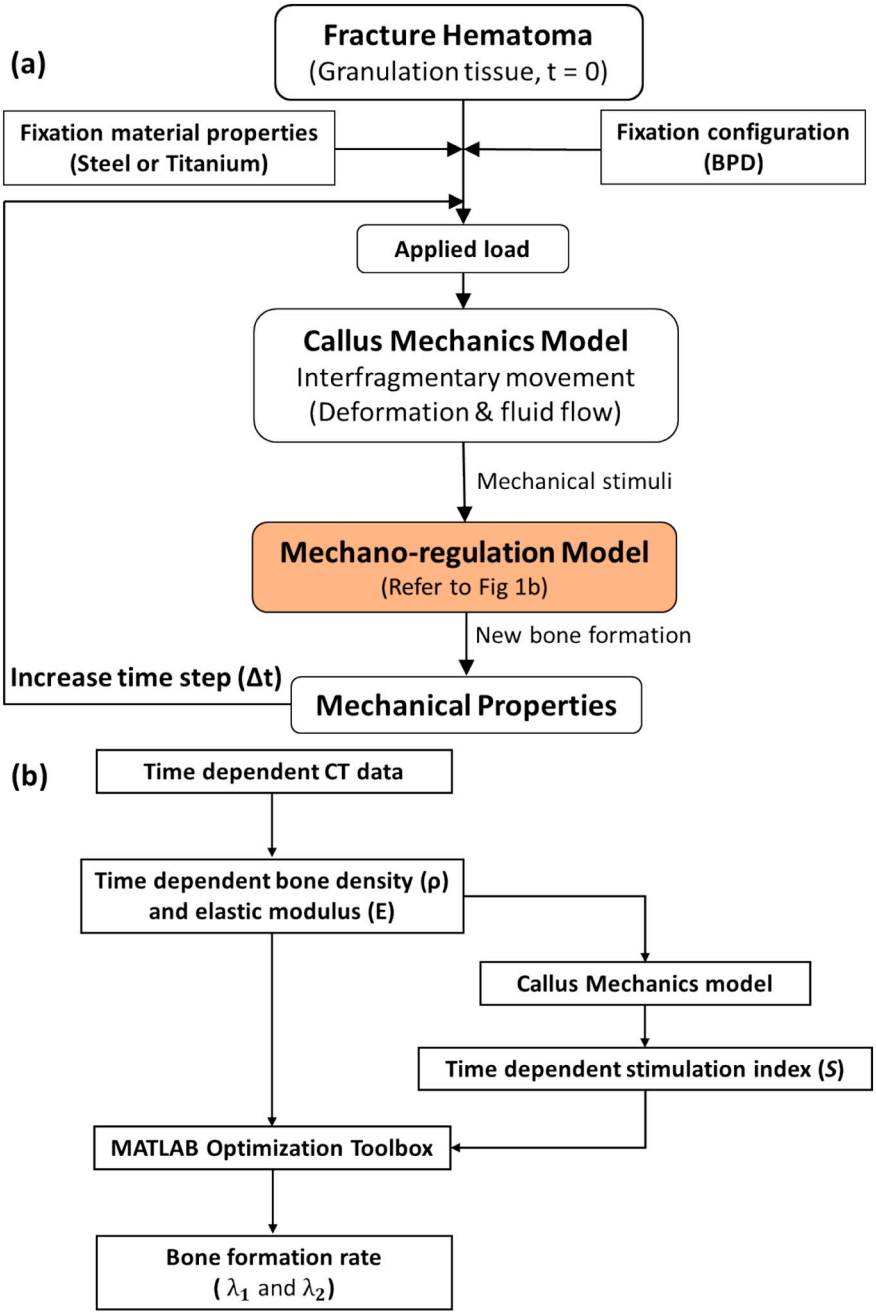

Fig. 1. (a) A schematic diagram for predicting mechanical stimuli mediated healing under different fixation conditions; and (b) Details of the mechano-regulation model proposed in this study

Miller et al. (2015) investigated how mechanical environment can regulate formation of various skeletal tissues during bone healing. Mechanical stimuli- induced strains were quantified and compared to the distribution of tissue phenotypes and found consistent relationships between strains experienced and mechanical stimulation with octahedral shear strain as determining factor. Similar conclusion had been derived by Isaksson et al. (2006) by comparing several mechanoregulation algorithms with in-vivo results. These studies demonstrate the effect of local mechanical stimuli on tissue formation leading to better understanding of the role of mechanical microenvironment in fracture healing. However, there hasn't been many studies that compare tissue formation rate through intramembranous and endochondral ossification process. This is largely due to the large number of complex processes occurring simultaneously during bone repair (Marsell and Einhorn, 2011). It has also been shown that the mechano-regulation in various stages of healing may differ from species to species (Checa et al., 2011).

Over the last decades, several mechano-regulation theories have been developed to quantify complex mechanical stimuli mediating the healing processes (Perren, 1979; Pauwels, 1960; Prendergast et al., 1997; Carter et al., 1998; Claes and Heigele, 1999). According to these theories, magnitude of stimuli determines the bone formation pathway under intramembranous ossification or endochondral ossification. In particular, the mechano-regulation model proposed by Prendergast et al. (1997) has been widely accepted (Isaksson et al., 2006) and further extended to predict cell differentiation/tissue formation during bone healing (Lacroix et al., 2002; Checa and Prendergast, 2009; Khayyeri et al., 2009; Isaksson et al., 2008; González-Torres et al., 2010; Reina-Romo et al., 2011; Miramini et al., 2017a; Zhang et al., 2017; Shanshan et al., 2019; Ganadhiepan et al., 2019a; Ganadhiepan et al., in press; Miramini and Yang, 2019). By treating callus as a poroelastic mixture in

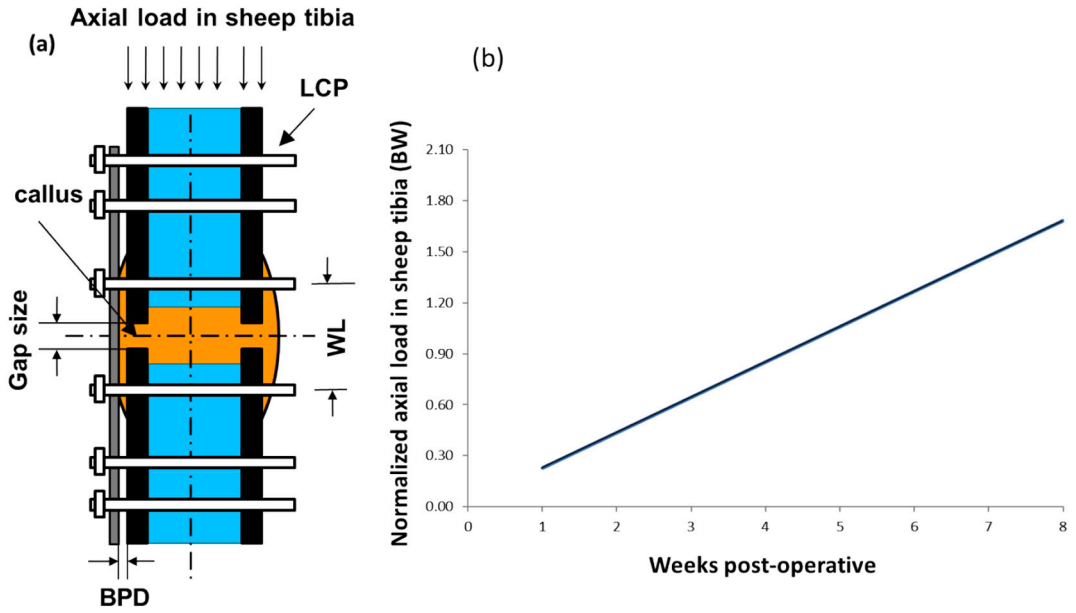

Fig. 2. (a) A schematic diagram of the Locking compression plate (LCP) system used in this study. The mechanical stiffness can be regulated by adjusting bone plate distance (BPD = 0 mm or 2 mm and defined as the distance between bone and fixation plate) and working length (WL = 35 mm and defined as the distance between two innermost screws); and (b) loading protocol where axial load in sheep tibia is normalized to its Body Weight (BW) and is assumed to increase linearly as healing progresses (Döbele et al., 2010; Grasa et al., 2010).

a computer model in conjunction with an in vivo experimental study, the authors have suggested that octahedral shear strain of the solid phase and interstitial fluid velocity relative to the solid phase are two important biophysical stimuli for mechano-regulatory pathway (Prendergast et al., 1997). Under low stimulus magnitude, the multi-potent mesenchymal stem cells (MSCs) differentiate directly into osteoblasts through the process of intramembranous ossification, while under moderate magnitude of stimulus, MSCs differentiate into chondrocytes through an endochondral ossification process. The current mechano-regulation models have limited capability of predicting the different bone formation rates under intramembranous and endochondral ossification processes.

The stiffness of bone fracture fixation is another important factor which can affect bone fracture healing processes. By adjusting the stiffness of a Locking Compression Plate (DePuy Synthes, Switzerland) through changing bone plate distance (BPD, defined as the distance between bone and fixation plate) and working length (WL, defined as the distance between two innermost screws), the study of Miramini et al. (2016a) demonstrated that the tissue differentiation behaviour in fracture callus could be significantly affected. It has also been shown that a relatively flexible fixation can potentially encourage bone healing (Augat et al., 1998).

Through developing numerical models in conjunction with animal experiments, the purpose of this study is to investigate the bone formation rate under intramembranous and endochondral ossification conditions. The models consider the spatial and time dependent changes in material properties of fractured bone as a result of the change of new bone content as healing progresses. In addition, the model has the capability of quantifying the healing outcomes under different fixation configurations and loading conditions.

2. Methods

2.1. Computational modelling

As shown in Fig. 1a, the proposed framework consists of a callus mechanics model and a mechano-regulation model. Detailed steps for developing the mechano-regulation model proposed in this study are shown in Fig. 1b. The total 8-week healing period is divided into several time-steps. Based on the configuration of fixation (LCP) system, axial force applied, and experimental bone density values determined each week, the callus mechanics model (refer to Section 2.1) is used to estimate the mechanical stimuli (fluid flow and deformation resulting from the interfragmentary movement) in callus for the corresponding week. Using this data for each healing week, bone formation rate and other parameters in the mechano-regulation model (refer to Section 2.2) are determined using a parameter optimization tool (refer to Fig. 1b).

For the numerical simulation (Refer to Fig. 1a), the callus mechanics model and mechano-regulation model are fully coupled, i.e. new mechanical properties of healing bone defined by the mechano-regulation model along with the applied load and fixation determines new mechanical stimuli for the callus mechanics model, and ultimately, new bone formation at the next time step, and forming a feedback loop. Further, the calibrated mechano-regulation model is then employed to improve the understanding of stiffness requirements of fixation systems used for fracture management (i.e. titanium LCP over stainless-steel LCP) and fracture union progression.

2.1.1. Callus mechanics model

The mechanical behaviour of fracture callus in Fig. 2 can be modelled by using a consolidation approach (Zhang et al., 2015; Zhang et al., 2008; Miramini et al., 2017b; Ghimire et al., 2018), which treats the callus as a porous media comprising an intrinsically solid phase (i.e. extracellular matrix) and an incompressible fluid phase. As at first estimate, the callus can be treated as an homogeneous material with a constant size and geometry (Garcia-Aznar et al., 2007; Gardnera et al., 2000). The relationship between the solid phase and fluid phase can be described as,

$$\nabla\cdot(\mathbf{v}^{s} - \kappa\nabla p) = 0 \tag{1}$$

$$-\nabla p + \nabla\cdot\sigma^{e} = 0 \tag{2}$$

where $\mathbf{v}^{s}$ is the solid phase velocity, p is the interstitial fluid pressure, σ^{e} is the elastic effective stress of solid matrix, and κ is the hydraulic permeability tensor.

As healing progresses, the elasticity and stiffness of callus increases

Table 1
Mean bone density values in HUs measured in near cortex (NC) and far cortex (FC) (BPD = 0 mm).

Sheep ID	Region	Week 1	Week 4	Week 6	Week 8	Remarks
#130	NC	277.4	675.1	688.5	723.5	Sacrificed 8
	FC	451.3	1020.7	1325.7	1504.6	wks post-op
#111	NC	254.3	604.6	949.2		Sacrificed 6
	FC	1066.6	1139.2	1182.7		wks post-op
#136	NC	326	604.3	610.8		Sacrificed 6
	FC	1398.8	1800.7	1859.2		wks post-op
#010	NC	533.1	850			Sacrificed 4
	FC	1098.3	1253.9			wks post-op
#007	NC	521.4				Sacrificed
	FC	1503.3				2wks post-op
Mean	NC	382.44	683.5	749.5	723.5	BPD = 0 mm
	FC	1103.66	1303.625	1455.87	1504.6	
SD	NC	134.766	115.88	177.26	NA	
	FC	410.425	344.78	356.54	NA	

(Moorcroft et al., 2001) with the increase in bone formation shown in experimentally determined bone density values in the callus (Refer to Tables 1 and 2). Therefore, it is reasonable to assume that the callus can be modelled based on the mechanical properties of the tissue formed during bone healing. While fracture callus is a heterogeneous mixture of granulation tissue, fibrocartilage tissue and bone tissue, bony tissue has the highest stiffness among these components (Leong and Morgan, 2008). Cartilage and fibrous tissue are indirectly incorporated in this study through experimentally determined bone formation occurring through cartilage calcification. Thus, the mechanical properties of newly formed bone can be correlated to the average bone density (ρ) (kg/m^3) across callus as follows:

$$E = 0.06\rho^{1.51} \tag{3}$$

where E is the elastic modulus (MPa) of fracture callus (Rho et al., 1995).

2.1.2. Mechano-regulation model

In the present study, it is assumed that the rate of bone formation during fracture healing can be expressed by "Hill Functions", which are commonly employed in biological systems (Alon, 2006). The total bone formation rate (B_p) is assumed to be composed of the basal bone formation rates (i.e. B_{p10} and B_{p20} in intramembranous and endochondral ossification, respectively) and mechanical stimuli induced bone formation rate, and is also limited by the maximum allowable bone density (ρ_m):

$$B_p = \begin{cases} \left(B_{p10} + \frac{\lambda_1 S^{n_1}}{K_1^{n_1} + S^{n_1}}\right)\left(1 - \frac{\rho}{\rho_m}\right) & 0 < S \le 1 \quad \text{(4a) Intramembranous ossification} \\ \left(B_{p20} + \frac{\lambda_2 S^{n_2}}{K_2^{n_2} + S^{n_2}}\right)\left(1 - \frac{\rho}{\rho_m}\right) & 0 < S \le 3 \quad \text{(4b) Endochondral ossification} \\ 0 & S > 3 \quad \text{(4c) No bone formation} \end{cases}$$

where mechanical stimulation index (S) is dependent on the octahedral shear strain of the solid phase (τ^s) and the interstitial fluid velocity (v^f, $\mu m/s$) obtained by governing Eqs. (1) and (2). That is,

$$S = \frac{\tau^s}{a} + \frac{v^f}{b} \tag{5}$$

where $a = 0.0375$ and $b = 3$ $\mu m/s$ are empirical constants (Prendergast et al., 1997). A relatively low magnitude of S at the early stage, i.e. $0 < S \le 1$ (Eq. (4a)) leads to intramembranous ossification, whereas a medium magnitude of S at the early stage, i.e. $1 < S \le 3$ (Eq. (4b)) results in endochondral ossification. In addition, an excessive simulation at the early stage of healing (i.e. $S > 3$) inhibits the healing (Eq. (4c)).

The parameters λ_1 and λ_2 are mechanical stimuli mediated bone formation rates in intramembranous and endochondral ossification, respectively. The "activation coefficients" K_1 and K_2 define the threshold of S which could lead to a significant increase in bone formation in intramembranous and endochondral ossification, respectively. The parameters n_1 and n_2 are the steepness of the Hill function (ranging from 1 to 6) in intramembranous and endochondral ossification, respectively.

2.2. Experimental study

Ten healthy skeletally mature cross-bred male sheep of 39–49 kg body-weight were obtained from the Charles Sturt University sheep farms. The animal study was conducted at the Veterinary Research Laboratory, Charles Sturt University, Australia. Sheep have been shown to be an ideal animal model for the study of fracture healing due to the comparable bone size and magnitude of applied loading to that of humans (Pearce et al., 2007; Rehman et al., 1995). This research was approved and conducted in accordance with, the Charles Sturt University (CSU) Animal Care and Ethics Committee (ACEC Approval Reference No. 14/031 and No. 15/099).

2.2.1. Study groups

The sheep with their sheep ID tag are presented in Tables 1 and 2. All

Table 2
Mean bone density values in HUs measured in (NC) and far cortex (FC) (BPD = 2 mm).

Sheep ID	Region	Week 1	Week 4	Week 6	Week 8	Remarks
#135	NC	256.9	401.2	604.8	1011.7	Sacrificed 8-weeks post-op
	FC	1053.4	1277.3	1696.2	1782.9	
#125	NC	398.4	435.9	515.7	787.3	Sacrificed 8-weeks post-op
	FC	378.5	1183.2	1226	1772.1	
#113	NC	287.5	537.9	857.6		Sacrificed 6-weeks post-op
	FC	907.2	1263.4	1400.7		
#035	NC	178.9	487.9			Sacrificed 4-weeks post-op
	FC	802.9	1063.9			
#037	NC	316.8				Sacrificed 2-weeks post-op
	FC	185.6				
Mean	NC	287.7	465.725	659.367	899.5	BPD = 2 mm
	FC	665.52	1196.95	1440.967	1777.5	
SD	NC	80.448	59.872	177.361	158.675	
	FC	367.5721	97.916	237.672	7.637	

animals underwent an acclimatisation period of at least 6 days and a clinical examination prior to admission to the study. The examination information including appetite, weight, body condition and appearance, cardiovascular and respiratory system, mobility, skin, teeth and mouth, ears, eyes and nose were recorded in the animal health report form and found to be normal.

2.2.2. Surgical technique and fracture stabilisation

A standard tibial transverse osteotomy with a 3-mm gap width was created using oscillating bone saw in mid diaphyseal tibia of healthy, under anaesthetic sheep. The SYNTHES Veterinary 3.5 mm broad stainless-steel LCP (VP4041.10–3.5 mm LCP Plate 10-hole, 131 mm) with 3.5 mm locking screws was used to stabilize the osteotomised tibia, maintaining 3 mm fracture gap. The sheep were divided into two groups, and each group of sheep were stabilized by either an LCP with a rigid configuration (i.e. BPD = 0), or with a relatively flexible configuration (i.e. BPD = 2 mm). Previous experimental study has illustrated that an increased BPD with a SYNTHES LCP increases inter-fragmentary movement in the fracture gap (Miramini et al., 2016a). For both animal groups, six locking screws placed on either side of plate holes 2, 4 and 5 from the plate centre on a plate working length of 35 mm. The sheep were then recovered in sternal recumbency and observed continuously until standing. In addition, to ensure the accuracy of the perspective of therapeutic effect, sheep were allowed to walk freely in a restricted area.

2.2.3. Post-operative care and follow-up examinations

For the first 7 days post-surgery, clinical observations were performed three times daily and analgesia was maintained throughout this period. The sheep were then anaesthetized every second week, beginning two weeks post-surgery. Since anaesthesia is known to induce hypotension that can restrict (or reduce) blood flow temporarily (Reich et al., 2005), the sheep were examined daily and no excessive hypotension was detected. The sheep underwent imaging examination and as per the predetermined post-surgical sacrifice the sheep were euthanized without recovery from the anaesthetic directly after their terminal CT scan.

2.2.4. Computed tomography (CT)

At 1-, 4-, 6- and 8-weeks post operation, bone mineral content in callus of right tibia was quantitatively determined by Densiscan 1000 scanner (Scanco Medical, Bassersdorf, Switzerland) which provides bone mineral density measurements in Hounsfield unit (HU) (Rho et al., 1995) That is,

$$\rho = 114 + 0.916HU \tag{6}$$

$$HU = 1000\frac{CT - CT_w}{CT_w - CT_a} \tag{7}$$

where ρ is bone density in kg/m^{3}and CT, CT_w and CT_a are the raw CT values of bone, saline and air, respectively. Previous experimental studies have shown that the radio densitometric measurements of bone strongly correlate with the histomorphometrically calculated bone values as a percentage of ossified tissue within the total volume (Augat et al., 1997). Therefore, the densiometric measurements recorded in Hounsfield units (HU) was used to determine the biomechanical properties of the callus (e.g. stiffness) in this study.

The CT machine was calibrated with a water phantom during each start-up cycle to ensure accurate image acquisition and images were taken directly prior to sacrifice. The relative degree of calcification is determined from the experimentally measured mean bone density value in HU normalized by that of intact sheep tibia in normal condition. Several control points were assessed using the "Outlier labelling rule" with a "k-value" of 1.5 as well as box-and whisker plot method to identify any potential interference from beam hardening artefact and prevent outlier masking.

Table 3
Material properties of bone and callus components used in this study.[a, b]

	Porosity	Poisson's ratio	Permeability (m^4/Ns)	Young's modulus (MPa)
Granulation tissue	0.8[a]	0.167[a]	10^{-14}[a]	0.05[b]
Marrow	0.8[a]	0.167[a]	10^{-14}[a]	2[a]
Cortical bone	0.04[a]	0.3[a]	10^{-17}[a]	2×10^4[a]

[a] Lacroix and Prendergast, 2002.
[b] McCartney et al., 2005.

Table 4
Material properties of the LCP used in this study (Stoffel et al., 2003b).

	Young's modulus (GPa)	Poisson's ratio
Stainless steel	220	0.34
Titanium	115	0.34

2.3. Numerical simulation

The tibia fracture model used in the computational simulation was created using our previous works (Miramini et al., 2016b). The fixation of screws to the bone is considered to have perfect bond in the model. Initially, the callus is filled with granulation tissue, and the material properties of bone components and the LCP are shown in Tables 3 and 4, respectively. Since cartilage and fibrous tissue in fracture callus are transient tissues which will ultimately be replaced by bone, their material properties were not explicitly included in Table 3. However, cartilage and fibrous tissue were indirectly modelled during the endochondral ossification process since experimentally determined bone density incorporates bone formation occurring through the cartilage calcification. The fractured limb is unable to bear total limb load during early stage of healing and patients are usually subjected to partial weight bearing after surgery. In a study conducted by Döbele et al. (2010), an initial loading of around 20% BW (for an average weight of 75 kg) was applied on tibial fractures supported by locking compression plate implants. Grasa et al. (2010) has further shown that load evolution during a gait cycle reaches over 1.2 times the BW of the animal. Further, graded increase in the fracture load was noted as fracture healing progressed (Browner et al., 2014). Therefore, an assumption was made that the applied axial force in sheep tibia increased linearly as healing progresses from around 20% of sheep body weight at early stage of healing to around 160% of BW in normal condition (Refer to Fig. 2b). To compare inter-fragmentary movement and degree of calcification between different configurations, same axial force is applied in both fixation configurations even though stiffness of fixator influences the application of external load. The numerical results were obtained by solving the governing equations using the commercial finite element software COMSOL MULTIPHYSICS v5.2 (COMSOL, n.d.). The cortical bone, marrow, fracture callus and locking plate fixation were meshed with 13,603, 6535, 14,335 and 15,683 s-order tetrahedral elements respectively, and the relative tolerance of 10 Pa for pressure and 10–4 m for displacement were employed for all calculations. The total Lagrangian formulation with material coordinate system was used to account for large deformation at early stage of healing when the callus is very soft (Levenston et al., 1998).

2.4. Parameter estimation for rate of bone formation

Our current experimental study provided two sets of time-dependent radio densitometry measurements of bone density in near and far cortex

Fig. 3. CT imaging of fractured bone. Mean bone density was evaluated in the area located in near cortex and far cortex by using Hounsfield unit (HU).

zones under different fixation conditions (i.e. BPD = 0 mm and BPD = 2 mm). The half cortex adjacent to fixation is referred to as near cortex and the opposite half-cortex as far cortex. First, the experimentally measured mean bone density (HU) in near and far cortex for each week (Section 2.2) and estimated mechanical stimulation index (S) from callus mechanics model (Section 2.1.1) for the corresponding week was used in the optimization process to determine parameters of bone formation rate (B_p) in Eq. (4). Then, a non-linear least squares and curve-fitting feature of MATLAB's optimization toolbox (MATLAB, 2015) was used and the values of parameters in Eqs. (4a) and (4b) were determined, i.e. new bone formation rates (λ_1 and λ_2), the activation coefficients (K_1 and K_2), and the steepness of the Hill function (n_1 and n_2), as well as the basal bone formation rates of new bone (B_{p10} and B_{p20}).

2.5. Statistics

The statistical analysis was performed on the experimental data using an analysis of variance (ANOVA) test and following variables were compared for significant differences (<0.05 level of confidence): near vs far cortex, changes over time, BPD = 0 mm vs BPD = 2 mm.

3. Results

3.1. Experimental results: Bone density values at near cortex and far cortex

As shown in Fig. 3, bone contents in near cortex and far cortex zones were quantitatively measured using CT. The experimentally measured mean bone density in HUs at 1-, 4-, 6- and 8-weeks post-operation are shown in Tables 1 and 2, and also presented in the experimental part of Fig. 4. Furthermore, Fig. 5 shows histological evaluations of new bone development using Masson's trichome staining at 8-weeks after animal sacrifice and removal of the fixation.

3.1.1. Statistical analysis

A significant difference was present between the mean bone density at near and far cortex ($p < 0.05$), which is consistent with the results of our previous study (Miramini et al., 2016a). Similarly, there was a significant difference between the change in mean bone densities over subsequent weeks. It showed that there is no significant difference in mean bone density between BPD = 0 mm and BPD = 2 mm. It should be mentioned that the statistical analysis between change in degree of calcification over subsequent weeks, and between BPD = 0 mm and BPD = 2 mm could only be performed at week 1, 4 and 6 due to small sample size during later stage of healing, especially at week 8.

3.2. Calibration of model parameters

Using experimental data, the values of model parameters were calibrated using an optimization process and the calibrated model parameters are shown in Table 5. The numerical model can reproduce experimentally observed change in bone content as shown in Fig. 4.

Fig. 6 shows the rate of relative degree of calcification induced by mechanical stimuli in intramembranous and endochondral ossification. The two sets of parameters were determined for intramembranous and endochondral ossification as shown in Table 5. The parameters $K_1 = 0.6$ (intramembranous ossification) and $K_2 = 1.0$ (endochondral ossification) indicate the thresholds of S which could trigger significant development in intramembranous and endochondral ossification, respectively. For example, K_1 is the "activation coefficient" which describes that the significant change in the rate of relative degree of calcification is triggered when the mechanical stimuli index (S) reaches to certain value (i.e. S = 0.6).

3.3. Effects of fixation stiffness on healing

It can be seen from Fig. 4 that the degree of calcification at far cortex is almost two-fold than that at near cortex under BPD = 0 mm and BPD = 2 mm. As locking compression plates are known to induce non-uniform healing across near cortex and far cortex (Stoffel et al., 2003a), effect of fixation stiffness on bone formation was numerically investigated by comparing near and far cortex using different fixation material, and the result is presented in Fig. 7. Under BPD = 0 mm, a titanium could increase the degree of calcification at near cortex more than 100% in the first two weeks in comparison to a stainless-steel LCP, and this enhancement gradually decreases with the increase of time (around 35–40% at 8-weeks post operation). However, titanium LCP showed little influence in final bone formation at far cortex.

4. Discussion

The non-uniform inter-fragmentary movement resulting from the LCP configuration (i.e. the inter-fragmentary movement at near cortex is much less than that at far cortex) could lead to spatially dependent mechanical stimuli across fracture site (Miramini et al., 2015; Ghimire et al., 2019; Bottlang, 2010; Miramini et al., 2014; Zhang et al., 2013). Due to this spatially dependent mechanical stimuli across fracture site, the relative degree of calcification in near cortex is different to that of far cortex zone (refer to Fig. 4), which is consistent with the clinical study that measured asymmetrical callus formation in distal femur fractures stabilized with locking plates (Lujan et al., 2010).

In this study, a higher mean bone density for BPD = 0 mm was observed at near and far cortex at week 1, 4 and 6 (refer to Tables 1 and 2) compared to BPD = 2 mm. However, this difference was not statistically significant, i.e. the change in bone plate distance from 0 mm to 2 mm had no significant difference on the mean bone density during fracture healing, even though lower bone plate distance has been regarded to provide better mechanical environment for healing (Stoffel et al., 2003a; Ahmad et al., 2007). Further, a higher mean bone density at week 8 was noted for BPD = 2 mm compared to BPD = 0 mm, which may indicate that a relatively flexible fixation improves healing process ultimately. However, statistical analysis could not be performed at week

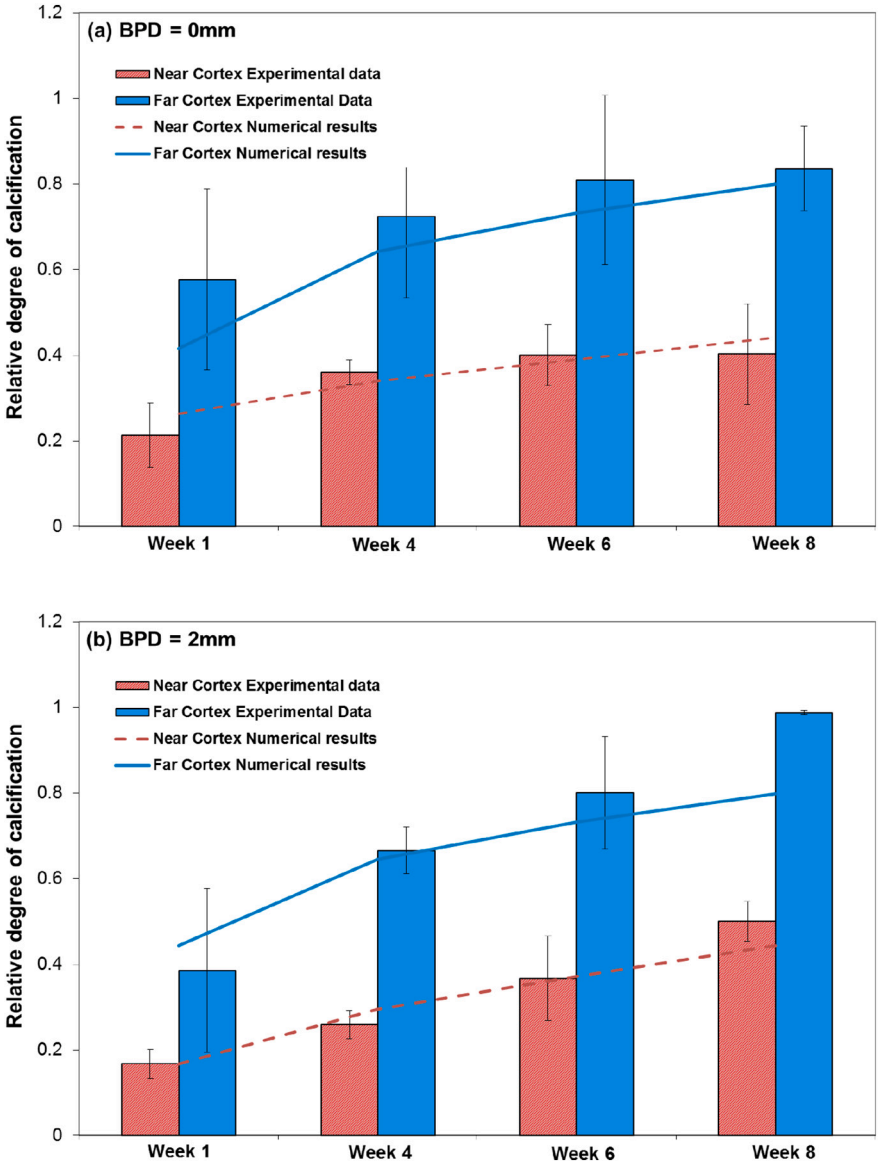

Fig. 4. Comparison of the numerical predictions to the animal experimental data. It can be seen that the experimental results are described remarkably well by numerical results using optimized model parameters.

8 due to small sample size and therefore, this result requires further investigation. Previous studies (Perren, 2002; Ganadhiepan et al., in press; Lujan et al., 2010; Henderson et al., 2008; Claes, 2011; Ganadhiepan et al., 2019a; Smith et al., 2018) have also indicated that flexible fixation can lead to better healing outcomes.

Previous experimental studies (Einhorn, 1998; Marsell and Einhorn, 2011; Augat et al., 1996) show that endochondral ossification occurs between fractured bone and external to periosteal callus (under relatively large strain), while intramembranous ossification occurs simultaneously in callus away from fracture site directly adjacent to distal and periosteal end of cortex (under relatively low strain). Under LCP fixation, the micro-motion in far cortex zone of callus is relatively larger than that in near cortex zone (Miramini et al., 2015; Bottlang, 2010; Lujan et al., 2010). Based on the interfragmentary strain profile from near cortex to far cortex for a similar LCP configuration (BPD = 2 mm & WL = 35.4 mm) by Miramini et al. (2013), endochondral ossification (2% to 10%) is most likely the dominated bone formation process in far cortex zone of callus, while intramembranous ossification (under 2%) is the dominated bone formation process in near cortex zone. This is also demonstrated in Figs. 4 and 5 which show a much higher time-dependent relative degree of calcification in far cortex zone than that in near cortex zone.

Fig. 6 shows that the bone formation under intramembranous and endochondral ossification has different thresholds (0.6 and 1 respectively) within the widely accepted magnitude range of mechanical stimuli index (S) by Prendergast et al. According to this theory, intramembranous ossification occurs within the stimuli index range of 0 to 1, and our study has further shown that there is a threshold (0.6) which triggers the significant bone formation under intramembranous ossification. Furthermore, a sensitivity analysis (Refer to Fig. 8) showed that the total bone formation rate is most sensitive to S, i.e. 10% increase in S resulted in 28% increase in the total bone formation rate (B_p). Therefore, this study demonstrates that, once a significant increase in bone formation is triggered, the bone formation rate in endochondral ossification (since it occurs between $1 < S < 3$) is generally higher than that in intramembranous ossification. This is consistent with other relevant

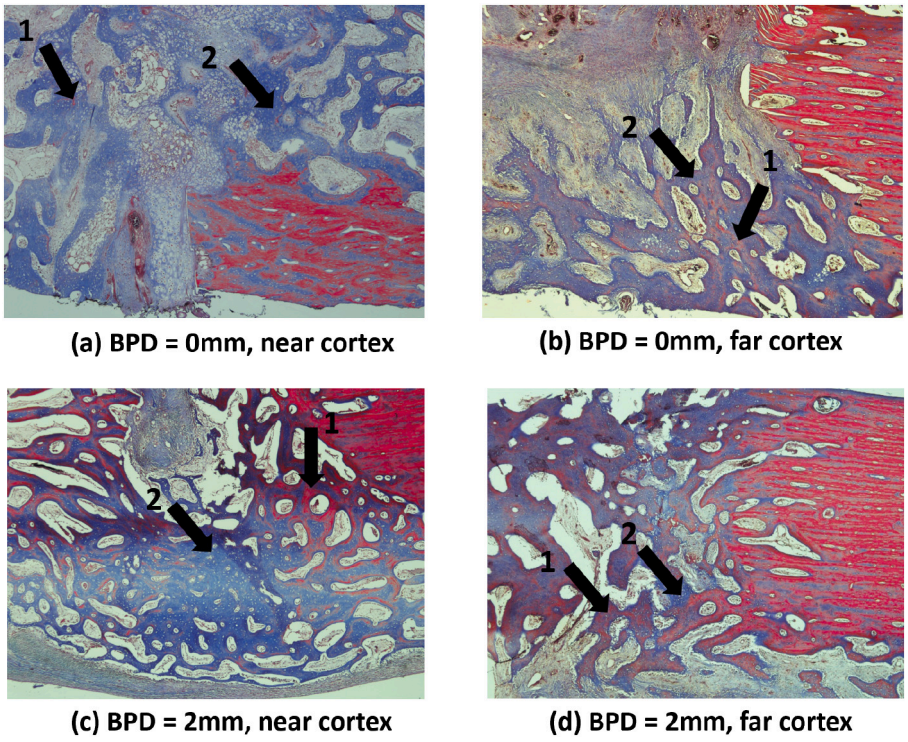

Fig. 5. Histological evaluations of new bone development using Masson's trichrome staining at 8-weeks after animal sacrifice and removal of the fixation. Arrow 1: new bone; Arrow 2: collagen.

Table 5
Values of parameters obtained by calibrating the experimental data; suffix 1 and 2 in parameters refer to intramembranous and endochondral ossification respectively.

Parameter	Value	Remarks
B_{p10} (basal bone formation rate)	8.96 mg/ml/day	Intramembranous ossification
B_{p20} (basal bone formation rate)	7.77 mg/ml/day	Endochondral ossification
λ_1 (new bone formation rate)	69.26 mg/ml/day	Intramembranous ossification
λ_2 (new bone formation rate)	142.9 mg/ml/day	Endochondral ossification
K_1 (activation coefficient)	0.6	Intramembranous ossification
K_2 (activation coefficient)	1.0	Endochondral ossification
n_1 (steepness of Hill function)	4.92	Intramembranous ossification
n_2 (steepness of Hill function)	2.0	Endochondral ossification

experimental studies (Woo et al., 1983; A et al., 1980; McKibbin and The biology of fracture healing in long bones, 1978), which suggested that endochondral ossification often results in faster bone union in comparison to intramembranous ossification.

Fig. 7 shows that the flexibility of the overall fixation system can be adjusted by not just changing the BPD and WL, but also by using less rigid materials (e.g. titanium) (Miramini et al., 2015). Further, with higher enhancement in near cortex compared to far cortex, titanium could lead to more uniform bone formation spatially. Thus, for the same fixation configuration, material properties of the fixation system could also significantly alter the healing outcomes.

An ANOVA test was performed for comparing bone density values between fixation configuration of BPD (0 & 2 mm) and a significant difference ($p < 0.05$ ANOVA) couldn't be established due to the small sample size. Further, current pilot study shows that at week #1, sheep #125 and #037 show an opposite trend of bone density (higher in the near cortex). This observation contrasts with the previous clinical and experimental studies who have reported smaller callus formation and interfragmentary movement at near cortex compared to far cortex in locking compression constructs (Bottlang, 2010; Bottlang et al., 2010; Richter et al., 2015). The observed irregularities in the experimental data should be further verified by large-scale experimental works.

4.1. Limitation

Owing to the large variations in the data, more experimental data is required to further validate these results. Since sheep were anaesthetized every two weeks, this might have affected fracture healing of sheep over time in a cumulative manner, including influence of anaesthesia and further experimental works should have one control group of sheep scanned only once after 8 weeks and then compared to the group that underwent anaesthesia and scanning throughout the healing. To simplify the complex problem, this study did not explicitly incorporate angiogenesis in the simulation. Being a pilot study, the model clearly needs to be further validated against future large experimental datasets, including studies considering the combined effect of biological and mechanical factors, including vascularity. Initial fracture response comprises of local activation of inflammatory factors, recruitment of inflammatory cells and macrophages, and coagulative response that stops further blood loss from ruptured vessels, forms hematoma and marks the onset of tissue repair and bone fracture healing (Chung et al., 2006). In our current model, only granulation tissue, which is a transition from hematoma, have been considered. An in-depth understanding the role of inflammatory response that stabilizes initial fracture site is needed by incorporating the mechanism into mechanobiological simulations as it plays pivotal role in governing healing outcomes. In addition, mechano-regulation rules governing the bone healing has been

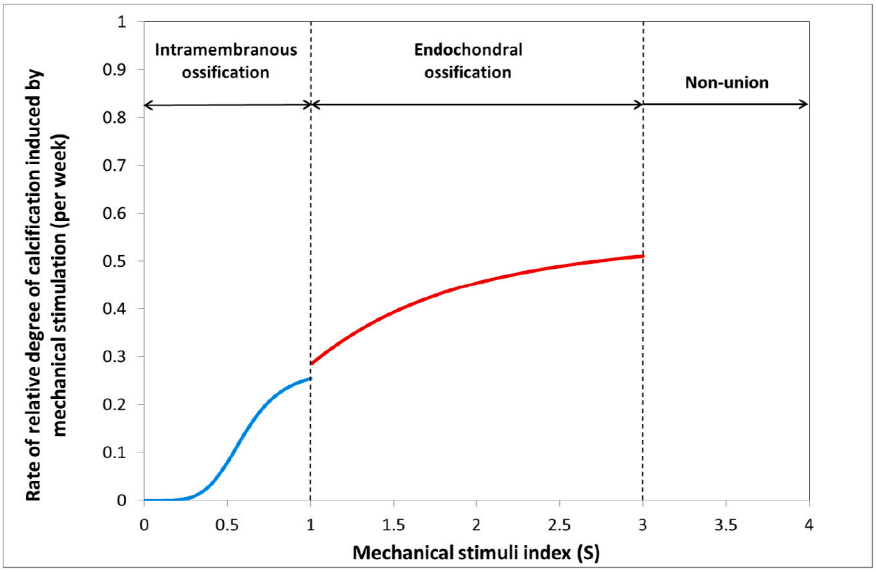

Fig. 6. Rate of relative degree of calcification (per week) induced by mechanical stimulation in intramembranous ossification ($0 < S \leq 1$) and endochondral ossification ($1 < S \leq 3$). It is assumed that the excessive S ($S > 3$) will lead to non-union.

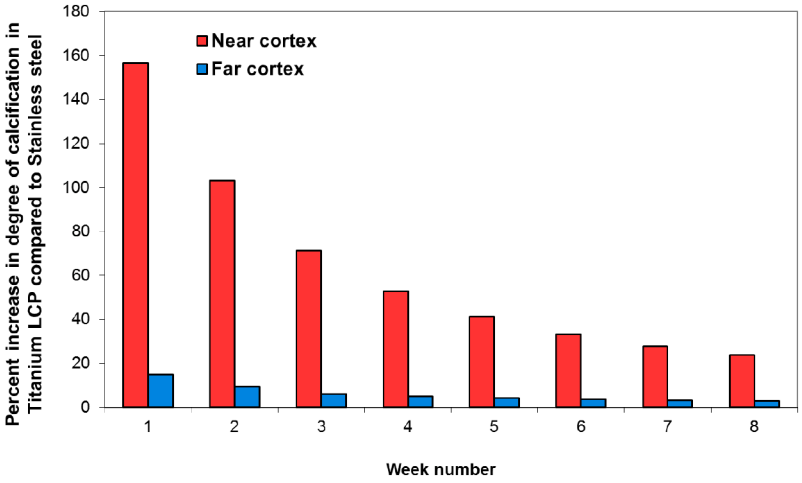

Fig. 7. Percent increase in degree of calcification as a function of time post-operation (weeks) by using titanium LCP relative to the control (i.e. Stainless steel LCP).

shown to differ from species to species and could also be changed in diseased conditions (e.g. osteoporosis) or elderly patients with reduced biological potential. The developed mechano-regulation model nevertheless provides a useful starting point for understanding bone fracture healing under different fixation configurations.

5. Conclusion

The purpose of this study was to investigate different bone formation rate under intramembranous and endochondral ossification processes during bone fracture healing by performing animal experiments in conjunction with theoretical modelling. The following were major findings:

- The mechanical stimuli mediated fracture healing showed that there are two unique sets of parameters of Hill Function which could describe the intramembranous and endochondral ossification.
- There are two different thresholds for intramembranous and endochondral ossification, which could trigger significant bone formation (i.e. Hill Function $K_1 = 0.6$ and $K_2 = 1$ obtained through optimization process).
- Once reaching thresholds that trigger significant bone formation, the rate of bone formation in endochondral ossification is generally higher than that in intramembranous ossification.
- There is a significant difference between relative degree of calcification under both fixation configuration (i.e. BPD = 0 mm and BPD = 2 mm) can be seen throughout the healing process ($p < 0.05$ ANOVA).
- An increase of the LCP flexibility by adjusting WL or BPD or using titanium LCP could potentially promote uniform bone formation across the fracture gap, ultimately better healing outcomes.

CRediT authorship contribution statement

Smriti Ghimire: Writing – original draft, Formal analysis, Software. **Saeed Miramini:** Methodology, Supervision, Writing – review & editing, Visualization, Software. **Glenn Edwards:** Investigation, Resources. **Randi Rotne:** Writing – review & editing, Resources. **Jiake Xu:** Validation. **Peter Ebeling:** Validation. **Lihai Zhang:** Conceptualization,

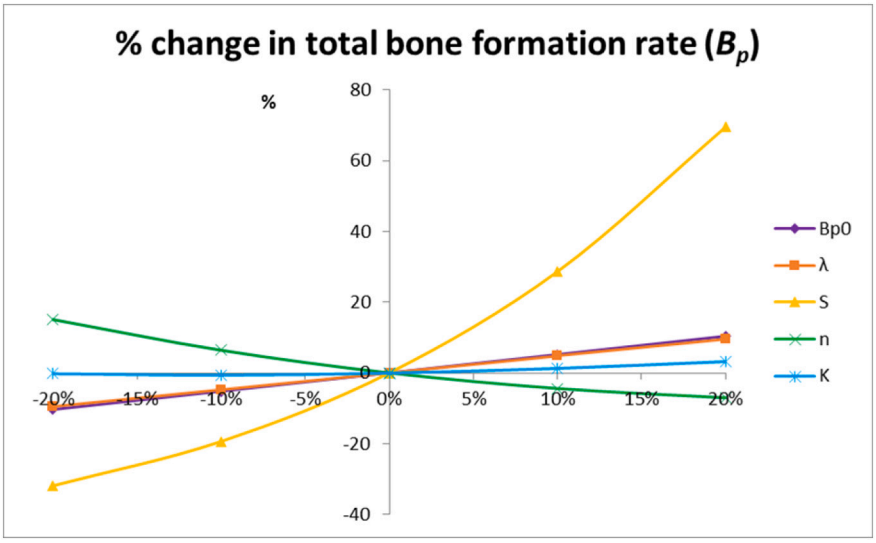

Fig. 8. Sensitivity analysis of the total bone formation rate (B_p) on depending parameters: basal bone formation rate (B_{p0}), new bone formation rate (λ), steepness of Hill's function (n), mechanical stimuli index (S) and activation coefficients (K).

Supervision, Writing – review & editing.

Acknowledgement

The authors would like to thank Johnson & Johnson Medical, The g (2015-2016), AOTRAUMA Asia Pacific (AOTAP14-02, 2014-2015) and AOA Research Foundation (Project grant 403) for their support.

References

A, A.S., et al., 1980. A quantitative comparative analysis of fracture healing under the influence of compression plating vs. closed weight-bearing treatment. Clinical Orthopaedics & Related Research 149, 232–239.
Ahmad, M., et al., 2007. Biomechanical testing of the locking compression plate: when does the distance between bone and implant significantly reduce construct stability? Injury 38 (3), 358–364.
Alon, U., 2006. An Introduction to Systems Biology. Chapman & Hall/CRC, Taylor & Francis Group.
Augat, P., et al., 1996. Early, full weightbearing with flexible fixation delays fracture healing. Clin. Orthop. Relat. Res. 328, 194–202.
Augat, P., et al., 1997. Quantitative assessment of experimental fracture repair by peripheral computed tomography. Calcif. Tissue Int. 60 (2), 194–199.
Augat, P., et al., 1998. Local tissue properties in bone healing: influence of size and stability of the osteotomy gap. J. Orthop. Res. 16 (4), 475–481.
Baker, C.E., et al., 2018. Bone fracture acute phase response—a unifying theory of fracture repair: clinical and scientific implications. Clinical Reviews in Bone and Mineral Metabolism 16 (4), 142–158.
Bottlang, M., et al., *Far cortical locking can improve healing of fractures stabilized with locking plates* The Journal of Bone & Joint Surgery, 2010. 92(7): p. 1652–1660.
Bottlang, M., et al., 2010. Effects of construct stiffness on healing of fractures stabilized with locking plates. JBJS **92** (Supplement_2), 12–22.
Browner, B.D., et al., 2014. Skeletal Trauma E-Book.
Carter, D.R., et al., 1998. Mechanobiology of skeletal regeneration. Clin. Orthop. Relat. Res. 355, S41–S55.
Checa, S., Prendergast, P.J., 2009. A mechanobiological model for tissue differentiation that includes angiogenesis: a lattice-based modeling approach. Ann. Biomed. Eng. 37 (1), 129–145.
Checa, S., Prendergast, P.J., Duda, G.N., 2011. Inter-species investigation of the mechano-regulation of bone healing: comparison of secondary bone healing in sheep and rat. J. Biomech. 44, 1237–1245.
Chung, R., et al., 2006. Roles of neutrophil-mediated inflammatory response in the bony repair of injured growth plate cartilage in young rats. J. Leukoc. Biol. 80 (6), 1272–1280.
Claes, L., 2011. Biomechanical principles and mechanobiologic aspects of flexible and locked plating. J. Orthop. Trauma 25, S4–S7.
Claes, L.E., Heigele, C.A., 1999. Magnitudes of local stress and strain along bony surfaces predict the course and type of fracture healing. J. Biomech. 32 (3), 255–266.
Claes, et al., 1995. Effect of dynamization on gap healing of diaphyseal fractures under external fixation. Clinical biomechanics (Bristol) **10** (5), 227–234.
COMSOL, Multiphysics® v. 5.2. COMSOL AB, Stockholm, Sweden.
Döbele, S., et al., 2010. The dynamic locking screw (DLS) can increase interfragmentary motion on the near cortex of locked plating constructs by reducing the axial stiffness. Langenbeck's Arch. Surg. 395 (4), 421–428.
Doblaré, M., Garcıa, J., Gómez, M., 2004. Modelling bone tissue fracture and healing: a review. Eng. Fract. Mech. 71 (13), 1809–1840.
Einhorn, T.A., 1998. The cell and molecular biology of fracture healing. Clin. Orthop. Relat. Res. 355, S7–S21.
Ganadhiepan, G., et al., 2019a. The effects of dynamic loading on bone fracture healing under Ilizarov circular fixators. J. Biomech. Eng. 141 (5), 051005.
Ganadhiepan, G., Miramini, S., Patel, M., Mendis, P., Zhang, L., 2019. Bone fracture healing under Ilizarov fixator: Influence of fixator configuration, fracture geometry, and loading. International journal for numerical methods in biomedical engineering 35 (6), e3199.
Garcia-Aznar, J.M., et al., 2007. Computational simulation of fracture healing: influence of interfragmentary movement on the callus growth. J. Biomech. 40 (7), 1467–1476.
Gardner, T., Mishra, S., 2003. The biomechanical environment of a bone fracture and its influence upon the morphology of healing. Med. Eng. Phys. 25 (6), 455–464.
Gardner, M.J., et al., 2006. In vivo cyclic axial compression affects bone healing in the mouse tibia. J. Orthop. Res. 24 (8), 1679–1686.
Gardnera, T.N., et al., 2000. The influence of mechanical stimulus on the pattern of tissue differentiation in a long bone fracture — an FEM study. J. Biomech. 33 (4), 415–425.
Gerstenfeld, L.C., et al., 2003. Fracture healing as a post-natal developmental process: molecular, spatial, and temporal aspects of its regulation. J. Cell. Biochem. 88 (5), 873–884.
Ghiasi, M., et al., 2017. Bone fracture healing in mechanobiological modeling: a review of principles and methods. Bone Reports 6, 87–100.
Ghimire, S., et al., 2018. Role of dynamic loading on early stage of bone fracture healing. Ann. Biomed. Eng. 1–17.
Ghimire, S., et al., 2019. Effects of dynamic loading on fracture healing under different locking compression plate configurations: a finite element study. J. Mech. Behav. Biomed. Mater. 94, 74–85.
González-Torres, L.A., et al., 2010. Influence of the frequency of the external mechanical stimulus on bone healing: a computational study. Med. Eng. Phys. 32, 363–371.
Grasa, J., et al., 2010. Monitoring in vivo load transmission through an external fixator. Ann. Biomed. Eng. 38 (3), 605–612.
Henderson, C.E., et al., 2008. Does locked plating of periprosthetic supracondylar femur fractures promote bone healing by callus formation? *Two cases with opposite outcomes*. The Iowa orthopaedic journal 28, 73.
Isaksson, H., et al., 2006. Comparison of biophysical stimuli for mechano-regulation of tissue differentiation during fracture healing. J. Biomech. 39 (8), 1507–1516.
Isaksson, H., et al., 2008. A mechano-regulatory bone-healing model incorporating cell-phenotype specific activity. J. Theor. Biol. 252 (2), 230–246.
Khayyeri, H., et al., 2009. Corroboration of mechanobiological simulations of tissue differentiation in an in vivo bone chamber using a lattice-modeling approach. J. Orthop. Res. 27 (12), 1659–1666.
Lacroix, D., Prendergast, P., 2002. A mechano-regulation model for tissue differentiation during fracture healing: analysis of gap size and loading. J. Biomech. 35 (9), 1163–1171.
Lacroix, D., et al., 2002. Biomechanical model to simulate tissue differentiation and bone regeneration: application to fracture healing. Med. Biol. Eng. Comput. 40 (1), 14–21.
Leong, P., Morgan, E., 2008. Measurement of fracture callus material properties via nanoindentation. Acta Biomater. 4 (5), 1569–1575.
Levenston, M., Frank, E., Grodzinsky, A., 1998. Variationally derived 3-field finite element formulations for quasistatic poroelastic analysis of hydrated biological tissues. Comput. Methods Appl. Mech. Eng. 156 (1), 231–246.
Lujan, T.J., et al., 2010. Locked plating of distal femur fractures leads to inconsistent and asymmetric callus formation. J. Orthop. Trauma 24 (3), 156–162.
Marsell, R., Einhorn, T.A., 2011. The biology of fracture healing. Injury 42 (6), 551–555.

MATLAB, 2015. MATLAB. The MathWorks, Inc.
McCartney, W., Donald, B.J.M., Hashmi, M.S.J., 2005. Comparative performance of a flexible fixation implant to a rigid implant in static and repetitive incremental loading. J. Mater. Process. Technol. 169 (3), 476–484.
McKibbin, B., 1978. The biology of fracture healing in long bones. J Bone Joint Surg Br 60-B (2), 150–162.
McKibbin, B., et al., 1978. The Journal of Bone and Joint Surgery **60** (2), 150. British volume.
Miller, G.J., Gerstenfeld, L.C., Morgan, E.F., 2015. Mechanical microenvironments and protein expression associated with formation of different skeletal tissues during bone healing. Biomech. Model. Mechanobiol. 14 (6), 1239–1253.
Miramini, S., Yang, Y., 2019. A probabilistic-based approach for computational simulation of bone fracture healing. Comput. Methods Prog. Biomed. 105011.
Miramini, S., et al., 2013. Computational simulation of the early stage of bone healing under different configurations of locking compression plates. Comput Methods Biomech Biomed Engin 18 (8), 900–913.
Miramini, S., et al. *Computational simulation of mechanical microenvironment of early stage of bone healing under locking compression plate with dynamic locking screws*. In *Applied Mechanics and Materials*. 2014. Trans Tech Publ.
Miramini, S., et al., 2015. Computational simulation of the early stage of bone healing under different locking compression plate configurations. Computer Methods in Biomechanics and Biomedical Engineering 18 (8), 900–913.
Miramini, S., et al., 2016a. The relationship between interfragmentary movement and cell differentiation in early fracture healing under locking plate fixation. Australas Phys Eng Sci Med 123–133.
Miramini, S., et al., 2016b. Influence of fracture geometry on bone healing under locking plate fixations: a comparison between oblique and transverse tibial fractures. Med. Eng. Phys. 38 (10), 1100–1108.
Miramini, S., et al., 2017a. The role of locking plate stiffness in bone fracture healing stabilized by far cortical locking technique. International Journal of Computational Methods 1850024.
Miramini, S., et al., 2017b. The spatio-temporal mechanical environment of healthy and injured human cartilage during sustained activity and its role in cartilage damage. J. Mech. Behav. Biomed. Mater. 74, 1–10.
Moorcroft, C.I., et al., 2001. Mechanical properties of callus in human tibial fractures: a preliminary investigation. Clin. Biomech. 16 (9), 776–782.
Morgan, E.F., et al., 2010. Correlations between local strains and tissue phenotypes in an experimental model of skeletal healing. J. Biomech. 43 (12), 2418–2424.
Moroni, A., et al., 2005. Current augmentation fixation techniques for the osteoporotic patient. Sandinavian Journal of Surgery 94, 103–109.
Pauwels, F., 1960. A new theory on the influence of mechanical stimuli on the differentiation of supporting tissue. The tenth contribution to the functional anatomy and causal morphology of the supporting structure. Z Anat Entwicklungsgesch 121, 478–515.
Pearce, A., et al., 2007. Animal models for implant biomaterial research in bone: a review. Eur Cell Mater 13 (1), 1–10.
Perren, S.M., 1979. Physical and biological aspects of fracture healing with special reference to internal fixation. Clinical Orthopaedics & Related Research 138, 175–196.
Perren, S.M., 2002. Evolution of the internal fixation of long bone fractures. Journal of Bone and Joint Surgery-British Volume 84 (8), 1093–1110.
Prendergast, P.J., Huiskes, R., Søballe, K., 1997. Biophysical stimuli on cells during tissue differentiation at implant interfaces. J. Biomech. 30 (6), 539–548.
Rehman, I., et al., 1995. Structural evaluation of human and sheep bone and comparison with synthetic hydroxyapatite by FT-Raman spectroscopy. J. Biomed. Mater. Res. 29 (10), 1287–1294.
Reich, D.L., et al., 2005. Predictors of hypotension after induction of general anesthesia. Anesth. Analg. 101 (3), 622–628.
Reina-Romo, E., et al., 2011. Effect of the fixator stiffness on the young regenerate bone after bone transport: computational approach. J. Biomech. 5 (5), 917–923.
Rho, J.Y., Hobatho, M.C., Ashman, R.B., 1995. Relations of mechanical properties to density and CT numbers in human bone. Med. Eng. Phys. 17 (5), 347–355.
Richter, H., et al., 2015. Dynamization at the near cortex in locking plate osteosynthesis by means of dynamic locking screws: an experimental study of transverse tibial osteotomies in sheep. J. Bone Joint Surg. (Am. Vol.) 97 (3), 208–215.
Rodan, G.A. and T.J. Martin, Therapeutic approaches to bone diseases. Science. **289** (5484): p. 1508–1514.
Shanshan, G., et al., 2019. Robot-assisted weight-bearing exercise for stroke patients with limited mobility. Journal of Low Frequency Noise, Vibration and Active Control 38 (2), 879–892.
Smith, D.W., et al., 2018. Articular Cartilage Dynamics. Springer.
Stoffel, K., et al., 2003a. Biomechanical testing of the LCP–how can stability in locked internal fixators be controlled? Injury 34, B11–B19.
Stoffel, K., et al., 2003b. Biomechanical testing of the LCP–how can stability in locked internal fixators be controlled? Injury 34, 11–19.
Vetter, A., et al., 2010. Temporal tissue patterns in bone healing of sheep. J. Orthop. Res. 28 (11), 1440–1447.
Woo, S., et al., 1983. Less rigid internal fixation plates: historical perspectives and new concepts. J. Orthop. Res. 1 (4), 431–449.
Zhang, L., et al., 2008. A fully coupled poroelastic reactive-transport model of cartilage. Molecular & Cellular Biomechanics 5 (2), 133–153.
Zhang, L., et al., 2013. The effects of flexible fixation on early stage bone fracture healing. International Journal of Aerospace and Lightweight Structures 3 (2), 181–189.
Zhang, L., et al., 2015. Time evolution of deformation in a human cartilage under cyclic loading. Ann. Biomed. Eng. 43 (5), 1166–1177.
Zhang, L., et al., 2017. Computational modelling of bone fracture healing under partial weight-bearing exercise. Med. Eng. Phys. 42, 65–72.